



# Synergistic effect of $\text{Ni(OH)}_2$ cocatalyst and CNT for high hydrogen generation on $\text{CdS}$ quantum dot sensitized $\text{TiO}_2$ photocatalyst

Junmei Wang<sup>a,b</sup>, Zhijian Wang<sup>a,\*</sup>, Zhenping Zhu<sup>a</sup>

<sup>a</sup> State Key Laboratory of Coal Conversion, Institute of Coal Chemistry, Chinese Academy of Sciences, Taiyuan, 030001, P.R. China

<sup>b</sup> University of Chinese Academy of Sciences, Beijing, 100049, P.R. China



## ARTICLE INFO

### Article history:

Received 30 September 2016

Received in revised form

28 November 2016

Accepted 4 December 2016

Available online 6 December 2016

### Keywords:

Hydrogen generation

$\text{Ni(OH)}_2$  cocatalyst

CNT

Charge transfer

Photocatalysis

## ABSTRACT

$\text{TiO}_2\text{-Ni(OH)}_2\text{/CNT/CdS}$  hybrid photocatalyst have been fabricated by a facile synthesis method under room temperature.  $\text{CdS}$  sensitized  $\text{TiO}_2$  hybrid photocatalysts with  $\text{Ni(OH)}_2$  and CNT cocatalysts anchored on  $\text{TiO}_2$  surface caused significant enhancement in photocatalytic  $\text{H}_2$  production rate in lactic acid aqueous solution under visible light irradiation. The optimized  $\text{TiO}_2\text{-Ni(OH)}_2\text{/CNT/CdS}$  shows high photocatalytic activity in  $\text{H}_2$  generation of  $12 \text{ mmol g}^{-1} \text{ h}^{-1}$  exceeding  $\text{TiO}_2\text{-Ni(OH)}_2\text{/CdS}$  and  $\text{TiO}_2\text{/CNT/CdS}$  which can be attributed to the combined effect of  $\text{Ni(OH)}_2$  and CNT. Photoluminescence and photoelectrochemical characteristics results demonstrated that the introduction of  $\text{Ni(OH)}_2$  and CNT displays synergistic effect in promoting the separation efficiency of the photoinduced electron-hole pairs. A scheme of charge transfer over the hybrid photocatalyst is proposed indicating the synergistic effect of  $\text{Ni(OH)}_2$  and CNT on promoting electron transport at the heterojunction surface between  $\text{TiO}_2$  and  $\text{CdS}$ . The performance of the stability of the  $\text{TiO}_2\text{-Ni(OH)}_2\text{/CNT/CdS}$  was tested in the presence of lactic acid under visible light irradiation. The system gives no loss in the hydrogen production after several recycling experiments confirming that the composite is stable and anti-photocorroded.

© 2016 Elsevier B.V. All rights reserved.

## 1. Introduction

Utilizing the solar resource in water splitting on semiconductor photocatalysts under visible light irradiation is an attractive environmental-friendly way to obtain clean hydrogen energy [1–3]. Considerable efforts have been focused on preparing efficient photocatalysts. Among the various semiconductors,  $\text{TiO}_2$  has received widely attention, because of its availability, nontoxicity, low cost, and stability against corrosion [4,5]. However, the photocatalytic ability is limited to UV region because of its wide band gap. To make use of the abundant visible light accounting for about 43% of the solar spectrum, appealing strategy is fabricating heterojunction materials by coupling of effective narrow band gap visible light driven semiconductors such as  $\text{CdS}$ ,  $\text{NiS}$ ,  $\text{MoS}_2$  with  $\text{TiO}_2$  [6–9]. Our previous work demonstrated that  $\text{CdS}$  combined with  $\text{TiO}_2$  was an efficient catalyst for  $\text{H}_2$  production [10]. Sargent reported that  $\text{CdS}$  quantum dot-sensitized solar cells exhibited energy conversion achieving at 7% [11]. Inorganic narrow gap semiconductor quantum dots (QDs) sensitized  $\text{TiO}_2$  systems have a great potential in improving photocatalytic activity. In comparison with common

semiconductor materials, quantum confined semiconductor dots acting as photosensitizers usually display some favorable advantages for photocatalytic hydrogen evolution in aqueous solution due to their excellent light absorption, more active sites, multiple excitons and long exciton lifetimes [12,13].  $\text{CdS}$  QDs are dispersed uniformly on the surface of the  $\text{TiO}_2$  support avoiding the aggregation of  $\text{CdS}$  quantum dots and providing with more active sites which is important in improving photocatalytic activity.

It is well known that the photogenerated electrons and holes recombine easily without loading cocatalyst on the semiconductors [14–17]. However, most cocatalysts of noble metals are scarce and expensive for practical applications [18,19]. Therefore, recently intensive studies on earth abundant nickel-based cocatalyst loaded on  $\text{CdS}$  in photocatalytic hydrogen production have been reported [20–23]. Further more, low-dimentional carbon nanomaterials possessing excellent photoelectron conducting properties can provide direct pathways for charge transport [24–27]. When combined with  $\text{TiO}_2\text{-Ni(OH)}_2\text{/CdS}$  heterojunctions, CNT can act as an electron shuttle inducing electron transfer from the conduction band of the  $\text{CdS}$  to  $\text{TiO}_2\text{-Ni(OH)}_2$ . Herein, we construct  $\text{CdS}$  sensitized  $\text{TiO}_2$  hybrid photocatalysts with  $\text{Ni(OH)}_2$  and CNT cocatalysts anchored on  $\text{TiO}_2$  surface and their enhancing  $\text{H}_2$  generation activity has been investigated in this research. This visible light responsive photocatalytic system is expected to provide some inspirations

\* Corresponding author.

E-mail address: [wangzhijian@sxic.ac.cn](mailto:wangzhijian@sxic.ac.cn) (Z. Wang).

on fabricating photocatalysts composites in improving solar-to-hydrogen efficiency.

## 2. Experimental section

### 2.1. Synthesis of $\text{TiO}_2\text{-Ni(OH)}_2$

All the reagents including  $\text{NaOH}$ ,  $\text{Ni}(\text{NO}_3)_2\cdot 6\text{H}_2\text{O}$ , CNTs (purchased from Tsinghua University of China),  $\text{CdCl}_2$ ,  $\text{NH}_3\text{H}_2\text{O}$ ,  $\text{NH}_4\text{Cl}$ ,  $\text{NH}_2\text{CSNH}_2$  and lactic acid were used without further purification. Degussa P25 was used as the source of  $\text{TiO}_2$ . 1.0 g P25 was dispersed in 50 mL 1.0 M  $\text{NaOH}$  aqueous solution and then a calculated amount of  $\text{Ni}(\text{NO}_3)_2\cdot 6\text{H}_2\text{O}$  dissolved in 5 mL  $\text{H}_2\text{O}$  was added, and the solution was stirred for 24 h at room temperature. Then the mixture was centrifuged, washed and dried in vacuum at 353 K for 24 h. The molar ratios of  $\text{Ni(OH)}_2$  to  $\text{Ni(OH)}_2\text{/TiO}_2$  were 0%, 0.5%, 1%, 2% and 100% respectively.

### 2.2. Synthesis of $\text{TiO}_2\text{-Ni(OH)}_2\text{/CNT/CdS}$

CNT was treated before use. 1 g CNT was dispersed in 100 mL  $\text{HNO}_3$  and stirred for 12 h, washed and dried in vacuum at 333 K for 12 h. After that the acidified CNT was suspended in water for further use. 0.1 g  $\text{Ni(OH)}_2\text{/TiO}_2$  photocatalyst was dispersed and stirred in a certain volume of 1 mg/mL CNT aqueous solution and then 10 mL 0.08 M  $\text{CdCl}_2$ , 10 mL 0.264 M  $\text{NH}_4\text{Cl}$ , 10 mL 0.56 M  $\text{NH}_2\text{CSNH}_2$  and 10 mL 0.92 M  $\text{NH}_3\cdot\text{H}_2\text{O}$  were added into the mixture in sequence. After stirred for 2 h at room temperature, the trace amount of CdS QDs sensitized  $\text{TiO}_2\text{-Ni(OH)}_2\text{/CNT}$  was centrifuged washed and dried at 333 K in vacuum for 12 h. For comparison, different amount of CdS contained in the composites were also synthesized.  $\text{TiO}_2\text{-Ni(OH)}_2\text{/CdS}$  and  $\text{TiO}_2\text{/CNT/CdS}$  were also prepared without adding  $\text{Ni(OH)}_2$  or CNT under the same experimental conditions.

## 3. Characterization

Transmission electron microscopy images were investigated on a high-resolution transmission electron microscopy (JEM-2100, 200 kV). X-ray diffraction (XRD) was performed using a Bruker D8 Advance X-ray powder diffractometer with  $\text{Cu K}\alpha$  ( $\lambda = 1.5406\text{\AA}$ ) radiation. The morphologies of the photocatalysts were investigated through field emission scanning electron microscopy (JSM-7001F, operated at 10 kV). Fourier transform infrared (FTIR) spectroscopy was performed with a Nicolet Magna-IR 550-II spectrometer, using KBr pellets. Raman spectra were recorded on a LABRAM-HR in a pulse laser with an excitation wavelength of 514 nm. UV-vis absorption spectroscopy was analyzed using a Shimadzu UV-3600 UV-vis-NIR spectrophotometer at room temperature.  $\text{BaSO}_4$  was used as the reflectance standard. Photoluminescence was measured on a fluorescence spectrometer (F-7000, Hitachi, Japan). The time resolved fluorescence decay spectra were obtained on a steady state and time resolved fluorescence spectrometers (FLSP920). X-ray photoelectron spectroscopy (XPS) was carried out on a Thermo ESCALAB 250 XPS spectrometer. The effect of sample surface charging was eliminated by shifting the XPS peak of carbon C1 s to 284.8 eV.

### 3.1. Photocatalytic measurements

Photocatalytic reactions were carried out in a flowing system (Ar gas with a flow rate at 1.5 L/h) with an inner-irradiation-type Pyrex reactor and a 300 w Xenon arc light source after filtering the UV light using a quartz water jacket filling with circulating cooling  $\text{NaNO}_2$  aqueous solution (1 M) to pass only visible light ( $\lambda > 400\text{ nm}$ ). Recycling  $\text{NaNO}_2$  solution was also utilized to main-

tain a constant reactor temperature at 298 K. 50 mg photocatalyst was suspended in 230 mL lactic acid aqueous solution (20 mL lactic acid, 210 mL water). Prior to irradiation, the reactor was purged with Ar gas for 25 min in order to replace air inside the solution. 1 mL of gas was sampled intermittently from the flowing system and then the amount of  $\text{H}_2$  evolved was analyzed by gas chromatography (Beifen-Ruili:SP-2100, MS-5A column, TCD, Ar carrier).

### 3.2. Electrochemical measurements

Photocurrent measurements were performed on an electrochemical workstation (CHI 660D Shanghai, China) using a standard three-electrode system with prepared samples as working electrode, a Pt foil as counter electrode and a standard calomel electrode in saturated KCl as reference electrode. The electrolyte was an aqueous solution containing 0.25 mM  $\text{Na}_2\text{S}$  and 0.25 mM  $\text{Na}_2\text{SO}_3$ . The working electrode were prepared as follows: photocatalyst (0.1 g) was stirred with 3 mL isopropyl alcohol for 24 h to form a slurry, and then the slurry was spin-coated onto FTO glass for further investigation.

## 4. Results and discussion

Fig. 1a shows the morphology of  $\text{TiO}_2\text{-Ni(OH)}_2\text{/CNT/CdS}$  photocatalyst. It can be clearly seen that  $\text{TiO}_2$  have an average diameter of 25 nm and small particles of CdS quantum dots with diameter about 5 nm closely adjacent to  $\text{TiO}_2$  particles (Fig. 1b). Especially, the doped CNT were distributed uniformly on the surface of the particles. However, the cocatalyst of  $\text{Ni(OH)}_2$  cluster were not found in the system. It can be ascribed to the primary crystal nucleus without ripening process to form regular particles. TEM images of the photocatalyst show that  $\text{TiO}_2$ , CdS and  $\text{Ni(OH)}_2$  are interacted with each other closely to form a composite.

X-ray photoelectron spectroscopy was employed to analyze the chemical composition of the photocatalyst. As shown in Fig. 1c, it is clear that the typical  $\text{Cd}3\text{d}$  peaks at 405.2 and 411.9 eV and  $\text{S}2\text{p}$  peaks at 161.5 and 162.7 eV corresponded to the CdS. The  $\text{C}1\text{s}$  peak at 284.6 eV mainly ascribed to the CNT added in the photocatalyst. The peaks of  $\text{Ti}2\text{p}$  located at about 459.0 and 464.4 eV implying in the form of  $\text{TiO}_2$  were also observed. Fig. 1d also shows the  $\text{Ni}2\text{p}$  signals observed at 856.1 and 874.0 eV, implying that the status of Ni element are major  $\text{Ni}^{2+}$  in  $\text{Ni(OH)}_2$  compounds.

Fig. 2a shows the XRD patterns of the  $\text{TiO}_2\text{-Ni(OH)}_2\text{/CNT/CdS}$  with different CdS contents. All samples exhibit the same characteristic diffraction peaks correspond to the  $\text{TiO}_2$  (JCPDS card no. 21-1272) and CdS (JCPDS card no. 41-1049). It is noteworthy that the typical diffraction peaks assigned to CNT can hardly been identified which could be ascribed to the main peak of CNTs at 25° is overlapped with the peak of  $\text{TiO}_2$ . The SEM image and corresponding SEM-EDX mapping (Fig. 2b and c) demonstrated the presence of Ti, O, Cd, S, C and Ni in the composite, and these elements are all well dispersed.

To confirm the composition of the composite and the interaction between  $\text{TiO}_2$ , CdS and CNT, FTIR spectra of the catalysts were compared in Fig. 3a. All the samples displayed the broad absorption at  $3400\text{ cm}^{-1}$  and  $1624\text{ cm}^{-1}$ , which is related to the bending vibrations of adsorbed water molecules. By comparing the composite with  $\text{TiO}_2$ , CdS, the two new peaks centered at  $1010\text{ cm}^{-1}$  and  $1396\text{ cm}^{-1}$  can be ascribed to the newly formed  $\text{Ti-O-C}$  [28,29] and C-S [30], respectively. The results indicated an evident chemical bond link between  $\text{TiO}_2$  and CNT, CdS and CNT.

Raman spectroscopy has also been employed to further provide structure information of the composite as shown in Fig. 3b. Prominent band at  $293\text{ cm}^{-1}$ ,  $589\text{ cm}^{-1}$  and  $881\text{ cm}^{-1}$  corresponding to CdS strongly indicated the CdS quantum dots were highly dispersed

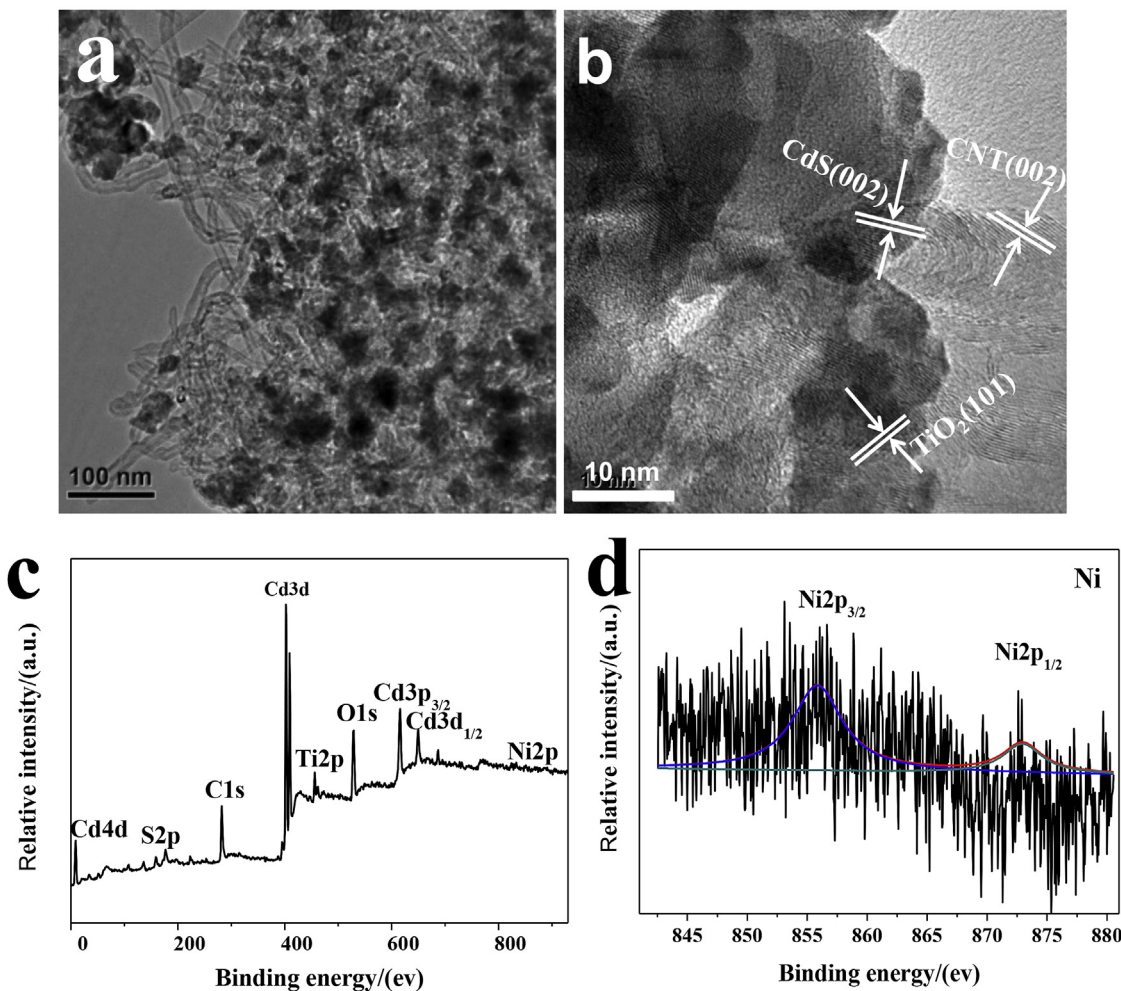


**Fig. 1.** TEM images of  $\text{TiO}_2\text{-Ni(OH)}_2\text{/CNT/CdS}$  (a,b) and XPS survey spectra of  $\text{TiO}_2\text{-Ni(OH)}_2\text{/CNT/CdS}$  and Ni 2p(c,d).

on the external surface of the composite. Compared with  $\text{TiO}_2$  and CNT, the vibration peak of  $144\text{ cm}^{-1}$  correspond to the  $\text{TiO}_2$  vibration mode, the D peak at  $1350\text{ cm}^{-1}$  and the G peak at  $1570\text{ cm}^{-1}$  all weakened, which is believed to derive from the CdS coating. The peak at  $1100\text{ cm}^{-1}$  can be attributed to the vibration of  $\text{Ni(OH)}_2$  [31].

The comparison of UV-vis diffuse reflectance spectra of  $\text{TiO}_2$ , CdS,  $\text{TiO}_2\text{/CdS}$ ,  $\text{TiO}_2\text{-Ni(OH)}_2\text{/CdS}$ ,  $\text{TiO}_2\text{/CNT/CdS}$  and  $\text{TiO}_2\text{-Ni(OH)}_2\text{/CNT/CdS}$  is displayed in Fig. 4. It is obviously that the absorption edges of pure  $\text{TiO}_2$  and CdS are estimated to be  $370\text{ nm}$  and  $517\text{ nm}$  respectively. After doped with  $\text{Ni(OH)}_2$  and CNT, no clear shift of the absorption edge for  $\text{TiO}_2\text{-Ni(OH)}_2\text{/CdS}$ ,  $\text{TiO}_2\text{/CNT/CdS}$  and  $\text{TiO}_2\text{-Ni(OH)}_2\text{/CNT/CdS}$  was observed in comparison to  $\text{TiO}_2\text{/CdS}$ , implying that  $\text{Ni(OH)}_2$  and CNT were not doped into the crystal structure of  $\text{TiO}_2$  and CdS. The result shows that  $\text{Ni(OH)}_2$  and CNT has no effect on optical properties of  $\text{TiO}_2\text{/CdS}$ . To ensure whether the  $\text{Ni(OH)}_2$  and CNT have any effect on photocatalytic activity, we conducted the  $\text{H}_2$  generation experiment.

Catalysts with different amount of CdS were firstly tested to evaluate the photocatalytic activity (Fig. S1). The  $\text{H}_2$  evolution rate of 10 wt% CdS loaded composite is higher than all other ones (5 wt%, 20 wt% and 40 wt% CdS). Control experiments were also conducted to investigate the effect of the amount of  $\text{Ni(OH)}_2$  and CNT on the photocatalytic  $\text{H}_2$  production activity. Pure  $\text{Ni(OH)}_2$  and CNT were used for comparison, no hydrogen were detected (Fig. 5). As shown in Fig. 5a, in the absence of  $\text{Ni(OH)}_2$ , the  $\text{H}_2$  production rate was  $1.01\text{ mmol g}^{-1}\text{ h}^{-1}$ , after loading with a small amount

of  $\text{Ni(OH)}_2$ , the  $\text{H}_2$  production rate was significantly enhanced to  $8.65\text{ mmol g}^{-1}\text{ h}^{-1}$  (0.5 wt%), about 9 times higher than the aforementioned sample. When the content was 1 wt%, the  $\text{H}_2$  production rate reached to the highest value of about  $12\text{ mmol g}^{-1}\text{ h}^{-1}$ . Further increasing amount to 2 wt%  $\text{Ni(OH)}_2$ , however, the  $\text{H}_2$  generation rate decreased to  $7.56\text{ mmol g}^{-1}\text{ h}^{-1}$ . A series of the  $\text{TiO}_2\text{-Ni(OH)}_2\text{/CNT/CdS}$  compounds with different doping amounts of CNT were also compared for the  $\text{H}_2$  production (Fig. 5b). For  $\text{TiO}_2\text{-Ni(OH)}_2\text{/CdS}$  catalyst without CNT, photocatalytic  $\text{H}_2$  production rate was  $5.36\text{ mmol g}^{-1}\text{ h}^{-1}$ . It was observed that the  $\text{H}_2$  generation rate increased with increasing doping amount of CNT. The highest  $\text{H}_2$  generation rate of  $12\text{ mmol g}^{-1}\text{ h}^{-1}$  was achieved at the amount of 4% CNT, further increasing the CNT amount led to a decrease of the  $\text{H}_2$  production. This can be ascribed to the shielding effect [32] in the presence of a large percentage of carbon materials.

To investigate the role of CNT and  $\text{Ni(OH)}_2$  for enhanced photocatalytic activity,  $\text{H}_2$  generation were compared as shown in Fig. 6a. The rate of  $\text{H}_2$  generation of  $\text{TiO}_2\text{-Ni(OH)}_2\text{/CNT/CdS}$  reaches to about  $12\text{ mmol g}^{-1}\text{ h}^{-1}$ , while for these in the absence of  $\text{Ni(OH)}_2$  or both CNT and  $\text{Ni(OH)}_2$ , the  $\text{H}_2$  evolution rate were decreased to  $5.36\text{ mmol g}^{-1}\text{ h}^{-1}$  and  $0.57\text{ mmol g}^{-1}\text{ h}^{-1}$  respectively, which is much lower than that of  $\text{TiO}_2\text{-Ni(OH)}_2\text{/CNT/CdS}$ , indicating that  $\text{Ni(OH)}_2$  is an excellent cocatalyst for promoting highly photocatalytic activity in hydrogen production. It can be seen that after doped with CNT, the hydrogen generation rate of  $\text{TiO}_2\text{-Ni(OH)}_2\text{/CNT/CdS}$  is about 2 times faster than that for  $\text{TiO}_2\text{-Ni(OH)}_2\text{/CdS}$ , which can be ascribed to the excellent electrical

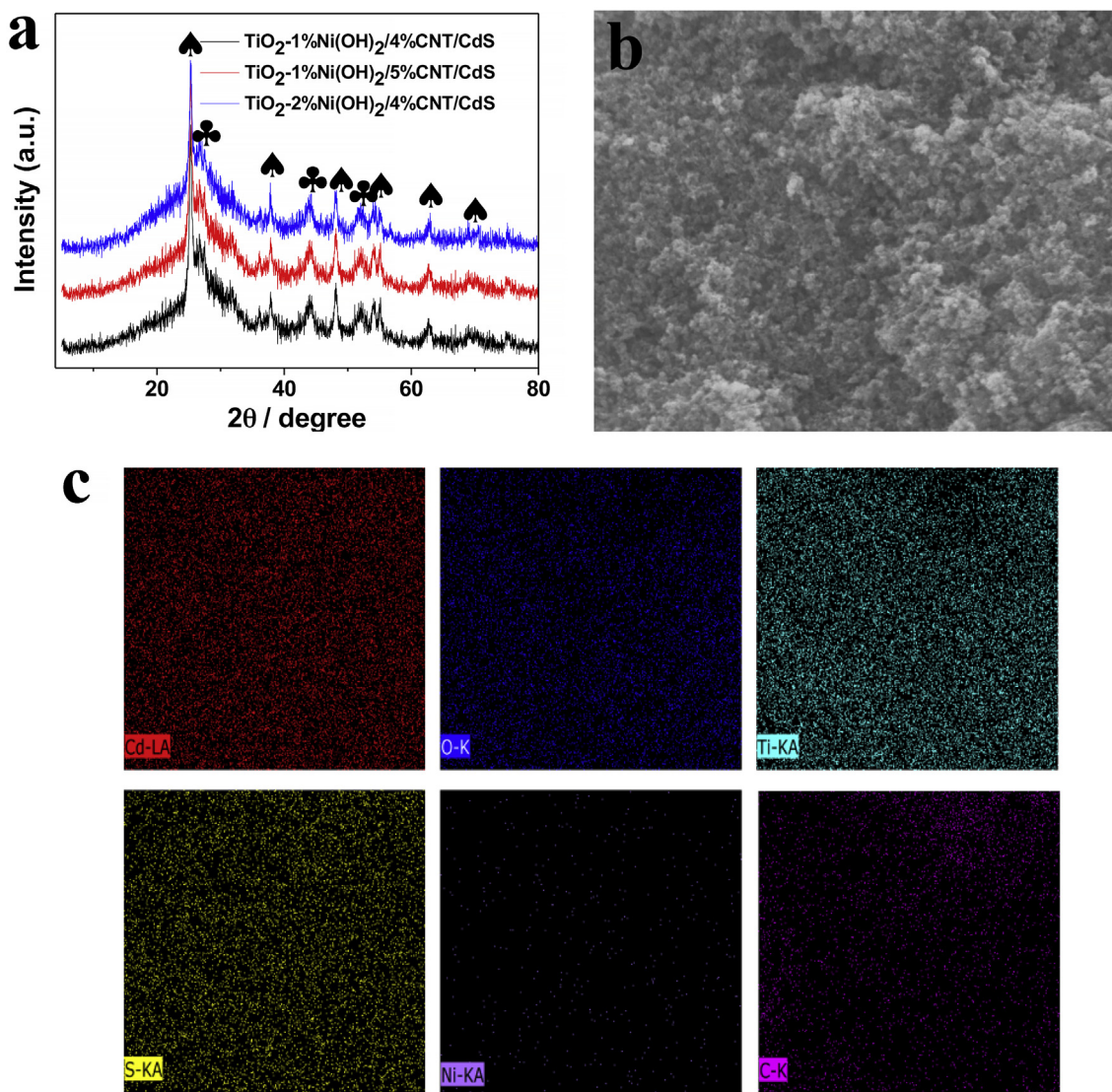


**Fig. 2.** Comparing XRD patterns of as-prepared optimized TiO<sub>2</sub>-Ni(OH)<sub>2</sub>/CNT/CdS with various CNT and Ni(OH)<sub>2</sub> content (a); SEM image and corresponding EDX mapping of TiO<sub>2</sub>-Ni(OH)<sub>2</sub>/CNT/CdS (b, c). ♠—corresponding to TiO<sub>2</sub>, ♣—corresponding to CdS.

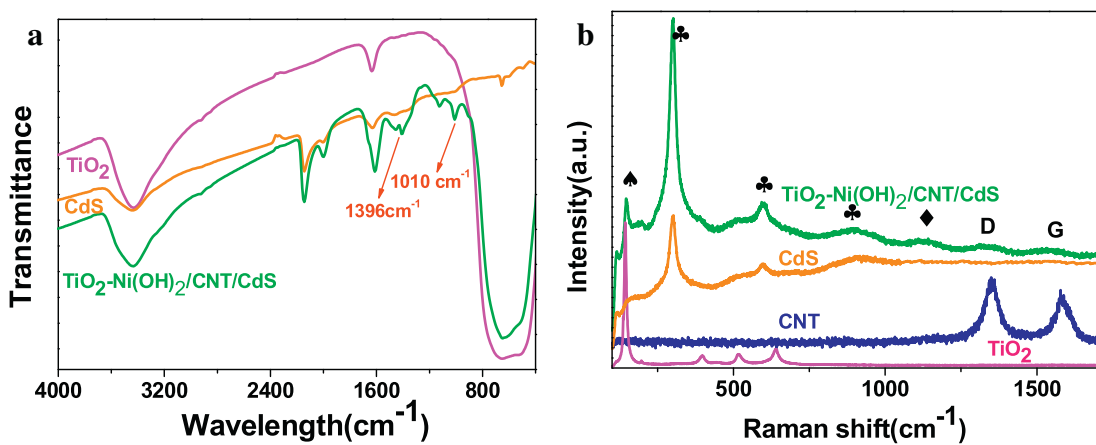


**Fig. 3.** FTIR spectra of TiO<sub>2</sub>, CdS and TiO<sub>2</sub>-Ni(OH)<sub>2</sub>/CNT/CdS (a) and Raman spectra of TiO<sub>2</sub>, CdS, CNT and TiO<sub>2</sub>-Ni(OH)<sub>2</sub>/CNT/CdS (b). ♠—corresponding to TiO<sub>2</sub>, ♣—corresponding to CdS, ♦—corresponding to Ni(OH)<sub>2</sub>.

conductivity of CNT, facilitating efficient charge carriers transport. To evaluate the stability of TiO<sub>2</sub>-Ni(OH)<sub>2</sub>/CNT/CdS photocatalyst,

recycling test was performed. As shown in Fig. 7, no significant decrease of H<sub>2</sub> production is observed after 5 cycling, which

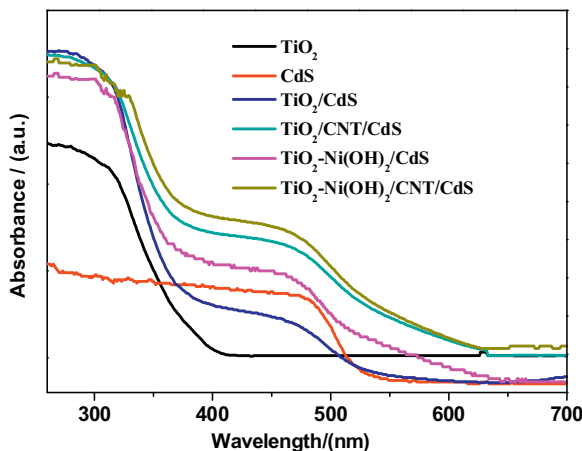


**Fig. 4.** UV-vis spectra of  $\text{TiO}_2$ ,  $\text{CdS}$ ,  $\text{TiO}_2/\text{CdS}$ ,  $\text{TiO}_2\text{-Ni(OH)}_2/\text{CdS}$ ,  $\text{TiO}_2/\text{CNT}/\text{CdS}$  and  $\text{TiO}_2\text{-Ni(OH)}_2/\text{CNT}/\text{CdS}$ .

indicates the good stability of  $\text{TiO}_2\text{-Ni(OH)}_2/\text{CNT}/\text{CdS}$  against photocorrosion. After the stability test, the composite was collected and further characterized by XRD, XPS and TEM as shown in Fig. S2, and all results give no obvious changes compared with that from the original catalysts.

To further verify the reason for high photoactivity, the transient photocurrent response of the samples were investigated and shown in Fig. 6b. It was clear that the  $\text{TiO}_2\text{-Ni(OH)}_2/\text{CNT}/\text{CdS}$  electrode exhibited higher photocurrent density than  $\text{TiO}_2/\text{CdS}$  and  $\text{TiO}_2\text{-Ni(OH)}_2/\text{CdS}$ , which indicates that by doping CNT and loading  $\text{Ni(OH)}_2$  cocatalyst, the recombination of electron-hole pairs is suppressed. Especially for the  $\text{TiO}_2/\text{CdS}$  catalyst without loading cocatalyst of  $\text{Ni(OH)}_2$  and CNT exhibits a drastically decreasing photocurrent density because of the rapid recombination of the photoinduced electrons and holes.

Photoluminescence spectra and time resolved photoluminescence spectra were used to explain the photogenerated carriers transfer process. Fig. 6c shows the PL spectrum, with emission bands at about 595 nm, compared with  $\text{TiO}_2/\text{CdS}$ , unloaded cocatalysts and CNT, emission intensity of  $\text{TiO}_2\text{-Ni(OH)}_2/\text{CdS}$  and  $\text{TiO}_2\text{-Ni(OH)}_2/\text{CNT}/\text{CdS}$  were drastically quenched after loading with  $\text{Ni(OH)}_2$ , indicating that  $\text{Ni(OH)}_2$  are very efficient traps for electrons photoinduced from  $\text{CdS}$  to  $\text{TiO}_2$ , which simultaneously suppresses the charge recombination process and enhance the photocatalytic activity. CNT provides pathway for the fluent electron transport, also suppressing the recombination of elec-

**Table 1**

Biexponential decay parameters for emission decay of  $\text{TiO}_2/\text{CdS}$ ,  $\text{TiO}_2\text{-Ni(OH)}_2/\text{CdS}$ , and  $\text{TiO}_2\text{-Ni(OH)}_2/\text{CNT}/\text{CdS}$ .

Samples	$a_1$	$\tau_1(\text{ns})$	$a_2$	$\tau_2(\text{ns})$	$\langle\tau\rangle(\text{ns})$
$\text{TiO}_2/\text{CNT}/\text{CdS}$	0.2564	0.418	0.0158	3.279	1.62
$\text{TiO}_2\text{-Ni(OH)}_2/\text{CdS}$	0.6282	0.216	0.0040	4.649	1.10
$\text{TiO}_2\text{-Ni(OH)}_2/\text{CNT}/\text{CdS}$	0.7029	0.201	0.0021	4.113	0.87

tron hole pairs [33]. Time resolved photoluminescence spectra for the samples provides a tool to evaluate their performance for electron-hole separation. As shown in Fig. 6d, the lifetime of  $\text{TiO}_2/\text{CdS}$ ,  $\text{TiO}_2\text{-Ni(OH)}_2/\text{CdS}$  and  $\text{TiO}_2\text{-Ni(OH)}_2/\text{CNT}/\text{CdS}$  is compared, and the average decay lifetimes are 1.62 ns, 1.10 ns and 0.87 ns respectively (Table 1). The lifetime of  $\text{TiO}_2\text{-Ni(OH)}_2/\text{CdS}$  and  $\text{TiO}_2\text{-Ni(OH)}_2/\text{CNT}/\text{CdS}$  is much shorter than that of  $\text{TiO}_2/\text{CdS}$ , indicating the effective charge transfer from  $\text{CdS}$  to  $\text{Ni(OH)}_2$ . The results demonstrated that  $\text{Ni(OH)}_2$  as an effective cocatalyst fixed on  $\text{TiO}_2$  significantly improve the charge injection from  $\text{CdS}$  to  $\text{TiO}_2$ , and ultimately into  $\text{Ni(OH)}_2$ . As compared to  $\text{TiO}_2\text{-Ni(OH)}_2/\text{CdS}$ , the lifetime of  $\text{TiO}_2\text{-Ni(OH)}_2/\text{CNT}/\text{CdS}$  gives no noticeable decrease. These indicate that CNT in the hybrids has little influence on the rate of charge injection process, however, it may play an important role in improving the charge separation, that is the CNT suppress the back electron transfer between the injected electrons in  $\text{Ni(OH)}_2$  and the holes in  $\text{CdS}$  [34]. This contributes to the better photocatalytic activity for hydrogen generation, from 5.36 to 11.87  $\text{mmol g}^{-1} \text{h}^{-1}$  (Fig. 6a).

Schematic illustration of the synergistic effect of  $\text{Ni(OH)}_2$  and CNT on enhanced photocatalytic  $\text{H}_2$  production activity mechanism for  $\text{TiO}_2\text{-Ni(OH)}_2/\text{CNT}/\text{CdS}$  hybrid is shown in Fig. 8. Visible light irradiation excited the electrons of the supported  $\text{CdS}$  QDs from the VB to CB. Then the electrons will be attracted immediately to the deposited  $\text{Ni(OH)}_2$  on  $\text{TiO}_2$  surface pass through CNT, and holes left to react with sacrificial agents of  $\text{Na}_2\text{S}/\text{Na}_2\text{SO}_3$ . The charge carrier separation was enhanced attributing to the excellent conductivity of CNT acting as a superhighway for the transport of the photogenerated electrons. Electrons trapped by  $\text{Ni(OH)}_2$  cocatalyst as the active reaction sites facilitated the reduction process of proton to hydrogen.

## 5. Conclusion

Simple and facile liquid chemistry synthetic method under room temperature was applied to prepare  $\text{TiO}_2\text{-Ni(OH)}_2/\text{CNT}/\text{CdS}$  hybrid photocatalyst. The photocatalytic  $\text{H}_2$  production performance of the typical  $\text{CdS}$  QDs sensitized  $\text{TiO}_2$ -based system was

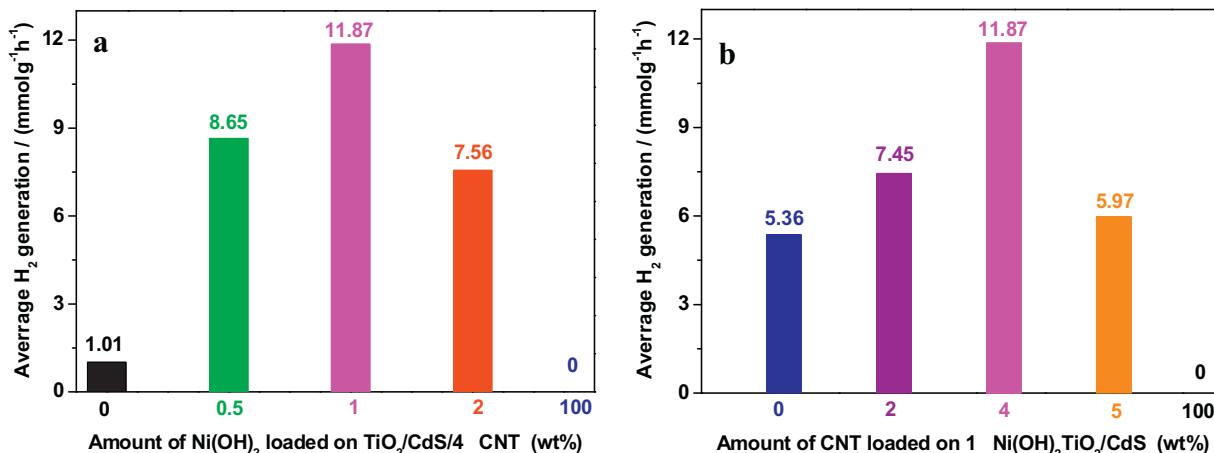


**Fig. 5.** Comparison of the photocatalytic activity of  $\text{TiO}_2\text{-Ni(OH)}_2/\text{CdS}$  under different conditions.

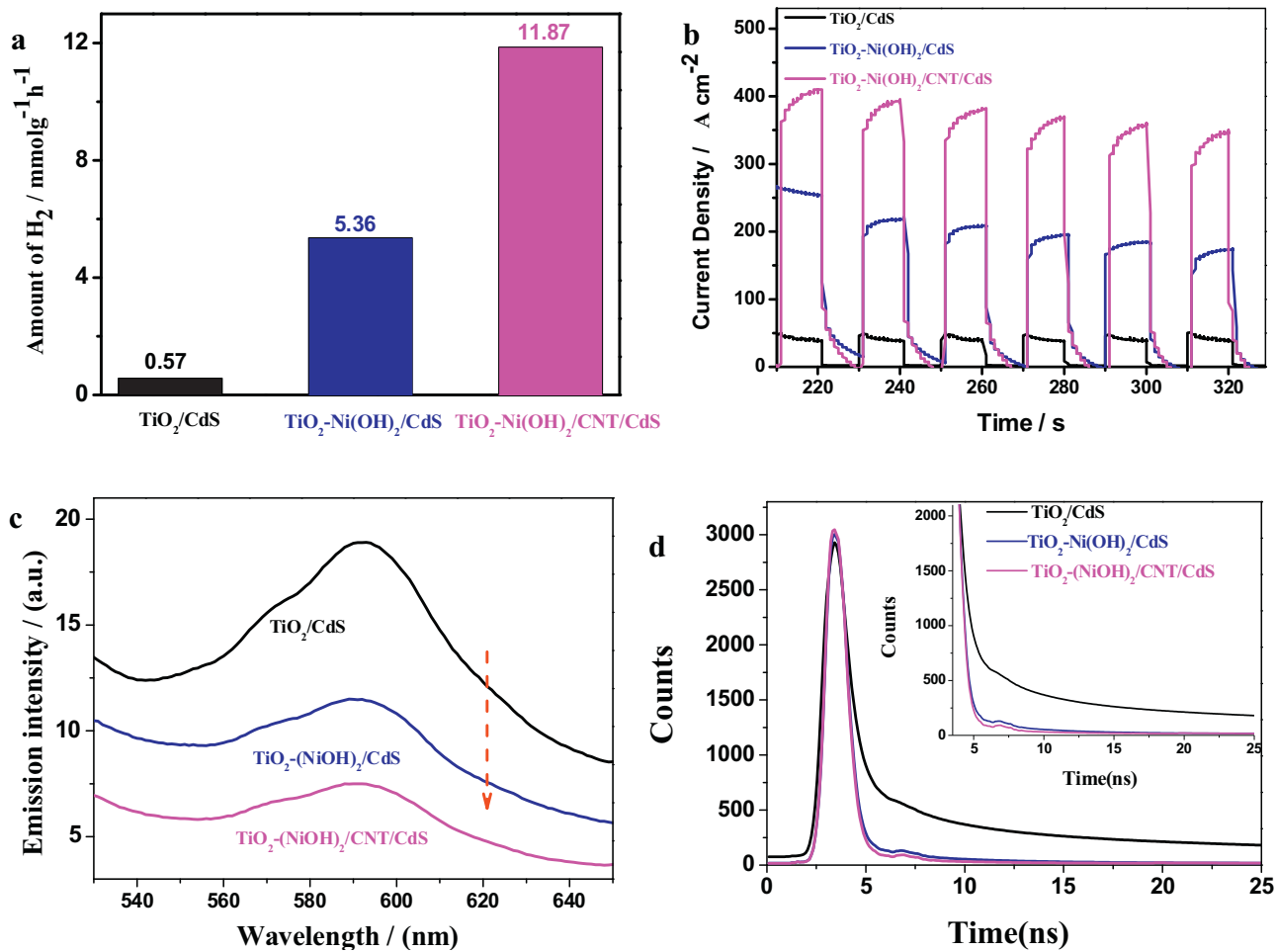


**Fig. 6.** (a) Comparison of the  $\text{H}_2$  evolution activity of the  $\text{TiO}_2/\text{CNT/CdS}$  with  $\text{TiO}_2\text{-Ni(OH)}_2/\text{CdS}$ , and  $\text{TiO}_2\text{-Ni(OH)}_2/\text{CNT/CdS}$ , in which the amount of CNT and  $\text{Ni(OH)}_2$  is optimized to 1 wt% and 4 wt% respectively. Light source 300 w Xe lamp ( $\lambda > 400$  nm). Reaction solution: 0.1 M  $\text{Na}_2\text{S}$ - $\text{Na}_2\text{SO}_3$  in 230 mL deionized water, Cat. 0.05 g. (b) Photocurrent response in  $\text{Na}_2\text{S}/\text{Na}_2\text{SO}_3$  aqueous solution with on-off visible light illumination (100 mW cm $^{-2}$ ) at 0.0 V vs NHE. (c) Photoluminescence spectra of  $\text{TiO}_2/\text{CNT/CdS}$ ,  $\text{TiO}_2\text{-Ni(OH)}_2/\text{CdS}$ , and  $\text{TiO}_2\text{-Ni(OH)}_2/\text{CNT/CdS}$ . (d) Time resolved PL emission decay of  $\text{TiO}_2/\text{CNT/CdS}$ ,  $\text{TiO}_2\text{-Ni(OH)}_2/\text{CdS}$ , and  $\text{TiO}_2\text{-Ni(OH)}_2/\text{CNT/CdS}$  (curves represent the kinetic fit using biexponential decay analysis) with an excitation wavelength of 450 nm.

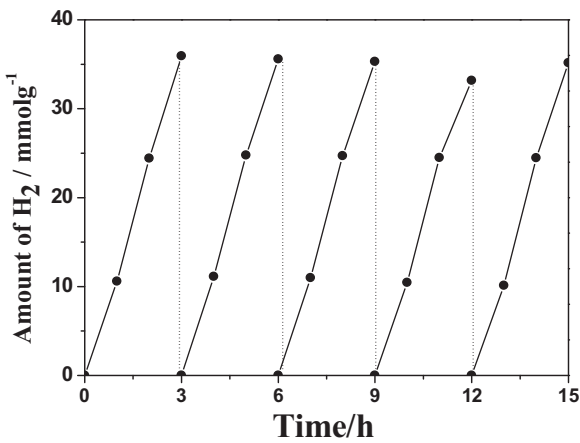


**Fig. 7.** Cycle test on  $\text{TiO}_2\text{-Ni(OH)}_2/\text{CNT/CdS}$  suspended in 230 mL 0.1 M  $\text{Na}_2\text{S}/\text{Na}_2\text{SO}_3$  aqueous solution bubbled with Ar per 3 h under irradiation of visible light.

promoted for the first time by the synergetic effect of  $\text{Ni(OH)}_2$  and CNT. The optimized photocatalytic activity is achieved over  $\text{TiO}_2\text{-Ni(OH)}_2/\text{CNT/CdS}$  with a rate of  $12 \text{ mmol g}^{-1} \text{ h}^{-1}$ . The excellent photocatalytic performance is mainly attributed to the facilitated charge separation and transfer at the interface of heterojunction

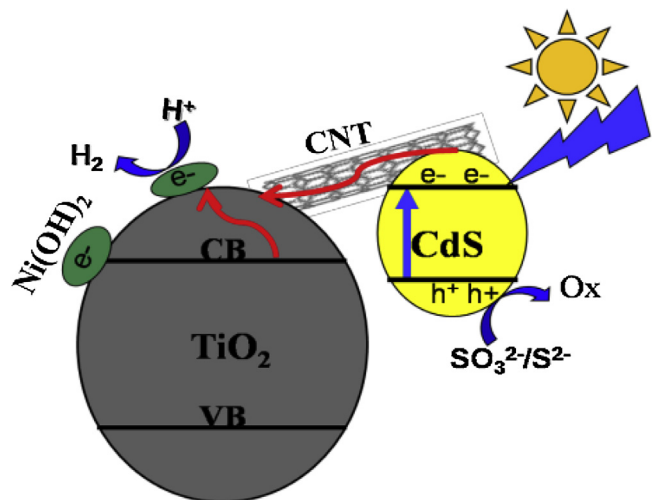


**Fig. 8.** Schematic illustration of the charge separation and electron transfer in the  $\text{TiO}_2\text{-Ni(OH)}_2/\text{CNT/CdS}$  system under visible light irradiation.

construction between  $\text{TiO}_2$  and  $\text{CdS}$  via coefficient effect of  $\text{Ni(OH)}_2$  and CNT.

In particular, the photocatalyst composition shows good stability and anti-photocorrosion under visible-light irradiation. The facile and environmentally synthesis technique can provide a way to produce other high catalytic H<sub>2</sub> generation via deposited with non-noble cocatalyst and doped with nanocarbon charge transfer materials.

## Acknowledgement

We acknowledge the financial support from National Natural Science Foundation of China (nos. U1510108 and 91545116).

## Appendix A. Supplementary data

Supplementary data associated with this article can be found, in the online version, at <http://dx.doi.org/10.1016/j.apcatb.2016.12.008>.

## References

- [1] Y.P. Yuan, L.W. Ruan, J. Barber, et al., Hetero-nanostructured suspended photocatalysts for solar-to-fuel conversion, *Energy Environ. Sci.* 7 (12) (2014) 3934–3951.
- [2] X. Li, J. Yu, J. Low, et al., Engineering heterogeneous semiconductors for solar water splitting, *J. Mater. Chem. A* 3 (6) (2014) 2485–2534.
- [3] J. Ran, J. Zhang, J. Yu, et al., ChemInform abstract: earth-abundant cocatalysts for semiconductor-based photocatalytic water splitting, *Chem. Soc. Rev.* 43 (22) (2014) 7787–7812.
- [4] Y. Ma, X. Wang, Y. Jia, et al., Titanium dioxide-based nanomaterials for photocatalytic fuel generations, *Chem. Rev.* 114 (19) (2014) 9987–10043.
- [5] C. Zhao, H. Luo, F. Chen, et al., A novel composite of TiO<sub>2</sub> nanotubes with remarkably high efficiency for hydrogen production in solar-driven water splitting, *Energy Environ. Sci.* 7 (5) (2014) 1700–1707.
- [6] Y. Zhu, C. Zhi, G. Tong, et al., Construction of hybrid Z-scheme Pt/CdS–TNTAs with enhanced visible-light photocatalytic performance, *Appl. Catal. B: Environ.* 163 (2015) 16–22.
- [7] J. Ran, J. Zhang, J. Yu, et al., Enhanced visible-light photocatalytic H<sub>2</sub> production by Zn<sub>x</sub>Cd<sub>1-x</sub>S modified with earth-abundant nickel-based cocatalysts, *Chemsuschem* 7 (12) (2014) 3426–3434.
- [8] C.T. Dinh, M.H. Pham, F. Kleitz, et al., Design of water-soluble CdS–titanate–nickel nanocomposites for photocatalytic hydrogen production under sunlight, *J. Mater. Chem.* 1 (42) (2013) 13308–13313.
- [9] B. Song, L. Wang, et al., Chemically exfoliated metallic MoS<sub>2</sub> nanosheets: a promising supporting co-catalyst for enhancing the photocatalytic performance of TiO<sub>2</sub> nanocrystals, *Nano Res.* 8 (1) (2015) 175–183.
- [10] J. Zhang, Z. Zhu, Y. Tang, et al., Titania nanosheet-mediated construction of a two-dimensional Titania/Cadmium sulfide heterostructure for high hydrogen evolution activity, *Adv. Mater.* 26 (5) (2014) 734–738.
- [11] A.H. Ip, S.M. Thon, S. Hoogland, et al., Hybrid passivated colloidal quantum dot solids, *Nat. Nanotechnol.* 7 (9) (2012) 577–582.
- [12] Y. Pan, T. Zhou, J. Han, et al., CdS quantum dots and tungsten carbide supported on anatase–rutile composite TiO<sub>2</sub> for highly efficient visible-light-driven photocatalytic H<sub>2</sub> evolution from water, *Catal. Sci. Technol.* 6 (7) (2015) 2206–2213.
- [13] Jiu-Ju Wang, Zhi-Jun Li, X.B. Li, et al., Inside cover picture: photocatalytic hydrogen evolution from glycerol and water over nickel-hybrid cadmium sulfide quantum dots under visible-light irradiation, *Chemsuschem* 7 (5) (2014) 1468–1475.
- [14] J. Yang, D. Wang, H. Han, et al., Roles of cocatalysts in photocatalysis and photoelectrocatalysis, *Acc. Chem. Res.* 46 (8) (2013) 1900–1909.
- [15] H. Yu, X. Huang, P. Wang, et al., Enhanced photoinduced-stability and photocatalytic activity of CdS by dual amorphous cocatalysts: synergistic effect of Ti(IV)-hole cocatalyst and Ni(II)-electron cocatalyst, *J. Phys. Chem. C* 120 (7) (2016) 3722–3730.
- [16] X. Zhou, J. Jin, X. Zhu, et al., New Co(OH)<sub>2</sub>/CdS nanowires for efficient visible light photocatalytic hydrogen production, *J. Mater. Chem. A* 4 (14) (2016) 5282–5287.
- [17] W. Zhang, Y. Wang, Z. Wang, et al., Highly efficient and noble metal-free NiS/CdS photocatalysts for H<sub>2</sub> evolution from lactic acid sacrificial solution under visible light, *Chem. Commun.* 46 (40) (2010) 7631–7633.
- [18] Lu Q., Yu Y., Ma Q., et al., 2D Transition-Metal-Dichalcogenide-Nanosheet-Based Composites for Photocatalytic and Electrocatalytic Hydrogen Evolution Reactions. 2016, 28, 10, 1917–1933.
- [19] S. Cao, Y. Chen, C.C. Hou, et al., Cobalt phosphide as a highly active non-precious metal cocatalyst for photocatalytic hydrogen production under visible light irradiation, *J. Mater. Chem. A* 3 (11) (2015) 6096–6101.
- [20] X. Yue, S. Yi, R. Wang, et al., Cadmium sulfide and nickel synergistic co-catalysts supported on graphitic carbon nitride for visible-light-driven photocatalytic hydrogen evolution, *Sci. Rep.* 6 (2016) 22268.
- [21] Z. Yan, X. Yu, Y. Zhang, et al., Enhanced visible light-driven hydrogen production from water by a noble-metal-free system containing organic dye-sensitized titanium dioxide loaded with nickel hydroxide as the cocatalyst, *Appl. Catal. B: Environ.* 160–161 (1) (2014) 173–178.
- [22] Z. Sun, H. Zheng, J. Li, et al., Extraordinarily efficient photocatalytic hydrogen evolution in water using semiconductor nanorods integrated with crystalline Ni<sub>2</sub>P cocatalysts, *Energy Environ. Sci.* 8 (9) (2015) 2668–2676.
- [23] Z. Chai, T.T. Zeng, L. Qi, et al., Efficient visible light-driven splitting of alcohols into hydrogen and corresponding carbonyl compounds over a Ni-modified CdS photocatalyst[J], *J. Am. Chem. Soc.* 138 (32) (2016) 10128–10131.
- [24] L. Wang, Z. Yao, F. Jia, et al., A facile synthesis of Zn<sub>x</sub>Cd<sub>1-x</sub>S/CNTs nanocomposite photocatalyst for H<sub>2</sub> production, *Dalton Trans.* 42 (27) (2013) 9976–9981.
- [25] M. Li, K. Chang, T. Wang, et al., Hierarchical nanowire arrays based on carbon nanotubes and Co<sub>3</sub>O<sub>4</sub> decorated ZnO for enhanced photoelectrochemical water oxidation, *J. Mater. Chem. A* 3 (26) (2015) 13731–13737.
- [26] N. Zhang, Y. Zhang, M.Q. Yang, et al., A critical and benchmark comparison on graphene-, carbon nanotube-, and fullerene-semiconductor nanocomposites as visible light photocatalysts for selective oxidation, *J. Catal.* 299 (2) (2013) 210–221.
- [27] N. Zhang, Y. Zhang, Y.J. Xu, Recent progress on graphene-based photocatalysts: current status and future perspectives, *Nanoscale* 4 (19) (2012) 5792–5813.
- [28] S. Wang, S. Zhou, Photodegradation of methyl orange by photocatalyst of CNTs/P-TiO<sub>2</sub>, under UV and visible-light irradiation[J], *J. Hazard. Mater.* 185 (1) (2011) 77–85.
- [29] U. Caudillo-Flores, J. Lara-Romero, J. Zárate-Medina, et al., Enhanced photocatalytic activity of MWCNT/TiO<sub>2</sub> heterojunction photocatalysts obtained by microwave assisted synthesis[J], *Catal. Today* 266 (2016) 102–109.
- [30] C. Zhang, Y. Lu, Q. Jiang, et al., Synthesis of CdS hollow spheres coupled with g-C<sub>3</sub>N<sub>4</sub> as efficient visible-light-driven photocatalysts[J], *Nanotechnology* 27 (35) (2016) 355402.
- [31] W. Zhou, X. Cao, Z. Zeng, et al., One-step synthesis of Ni<sub>3</sub>S<sub>2</sub> nanorod@Ni(OH)<sub>2</sub>nanosheet core–shell nanostructures on a three-dimensional graphene network for high-performance supercapacitors[J], *Energy Environ. Sci.* 6 (7) (2013) 2216–2221.
- [32] Q. Li, B. Guo, J. Yu, et al., Highly efficient visible-light-driven photocatalytic hydrogen production of cdS-cluster-decorated graphene nanosheets, *J. Am. Chem. Soc.* 133 (28) (2011) 10878–10884.
- [33] W.K. Jo, N.C.S. Selvam, Fabrication of photostable ternary CdS/MoS<sub>2</sub>/MWCNTs hybrid photocatalysts with enhanced H<sub>2</sub> generation activity, *Appl. Catal. A Gen.* 525 (2016) 9–22.
- [34] P. Brown, A. Kensuke Takechi, P.V. Kamat, Single-walled carbon nanotube scaffolds for dye-sensitized solar cells, *J. Phys. Chem. C* 112 (12) (2008) 4776–4782.